

## Towards V-based high-entropy alloys for nuclear fusion applications

P.J. Barron<sup>a,\*</sup>, A.W. Carruthers<sup>a</sup>, J.W. Fellowes<sup>a</sup>, N.G. Jones<sup>b</sup>, H. Dawson<sup>c</sup>, E.J. Pickering<sup>a</sup>

<sup>a</sup> Department of Materials, University of Manchester, Oxford Road, Manchester M13 9PL, UK

<sup>b</sup> Department of Materials Science and Metallurgy, University of Cambridge, 27 Charles Babbage Road, Cambridge CB3 0FS, UK

<sup>c</sup> Culham Centre for Fusion Energy, Abingdon OX14 3DB, UK



### ARTICLE INFO

#### Article history:

Received 9 August 2019

Revised 17 September 2019

Accepted 18 September 2019

#### Keywords:

High-entropy alloys

Refractory metals

Transition metals

### ABSTRACT

By mixing elements with favourable nuclear activation properties to create high-entropy alloys, it may be possible to create a material that can withstand a nuclear fusion environment while minimising the radioactive waste produced. Such a material could be used in the extreme thermal and irradiation conditions of a fusion blanket. A suite of previously unexplored V–Cr–Mn and V–Cr–Mn–Ti alloys have been fabricated then homogenised and the resultant microstructures and phases were characterised. Results demonstrate that single-phase body centred cubic solid solution microstructures can be formed in highly-concentrated alloys incorporating low-activation elements, which is promising for a fusion alloy development standpoint.

© 2019 Acta Materialia Inc. Published by Elsevier Ltd.

This is an open access article under the CC BY license. (<http://creativecommons.org/licenses/by/4.0/>)

Nuclear fusion offers an alternative low-carbon energy source with potentially abundant fuel. However, fusion reactors must minimise the amount of harmful radioactive waste they produce in order to be considered a truly green energy source. This criteria necessitates the use of low-activation alloys, made from elements that will not remain radioactive for extended periods of time after exposure to fusion neutrons.

The structural material of a fusion reactor blanket also has to face a variety of hostile conditions, including: extremes of neutron irradiation and temperature, transient loading from plasma instabilities, and corrosion from coolant systems [1]. These conditions necessitate the use of a material that is sufficiently strong, with good irradiation and creep resistance. The blanket will also require thousands of tons of material, precluding the use of extremely costly or scarce elements as significant alloying additions, or alloys that cannot be processed on large scales. Further restrictions are imposed by the aforementioned desire to use low-activation elements. Table 1 shows the calculated time taken for selected elements to reach UK low-level waste (LLW) ( $<4$  MBq kg<sup>-1</sup> alpha radiation and  $<12$  MBq kg<sup>-1</sup> combined gamma and beta radiation) after 5 years of pulsed operation in the DEMO reactor divertor body [2]. Although the divertor will be exposed to a greater fluence of neutrons, these values are still representative of their relative activities when used in a fusion blanket. It is apparent

that certain elements such as Ni or Zr which are commonly used for nuclear structural applications would be unacceptable from a waste-management perspective.

Research efforts for fusion structural materials have been primarily focused on reduced activation ferritic–martensitic (RAFM) steels and vanadium alloys [3–5]. However, RAFM steels have a relatively low maximum operating temperature, limited by creep [6]. Their oxide dispersion strengthened counterparts offer improved high temperature performance but large scale processing is still an issue [4]. V-based alloys containing other elements as minor ( $<10$  at%) additions have been explored as an alternative to steels for fusion blanket applications[3]. However, high-entropy alloys (HEAs) containing multiple low-activation elements have received very little attention. A recent study by Ayyagari et al. [7] examined the Ta–Ti–V–Zr–X system, but here we avoid Zr owing to its activation properties listed in Table 1. Investigation of more concentrated alloys covering unexplored compositional space may yield materials that are more processable and have enhanced properties in comparison to the more conventional alloys. Other HEAs have shown surprising toughness [8] and irradiation swelling properties [9], so it is hoped that this work may form the basis for developing fusion alloys with improved properties such as a larger operating temperature window or easier processing.

Due to the favourable activation properties of their constituent elements, alloys in the V–Cr–Mn ternary and V–Cr–Mn–Ti system were investigated. The nominal compositions are shown in Table 2. V and Cr were chosen because of their high melting points, which

\* Corresponding author.

E-mail address: [paul.barron@manchester.ac.uk](mailto:paul.barron@manchester.ac.uk) (P.J. Barron).

**Table 1**

Calculated time taken to reach UK LLW for selected elements after use in a DEMO reactor divertor. Elements used in this study have been highlighted. Data taken from [2].

| Element   | Time to LLW/yr    | Element   | Time to LLW/yr    | Element | Time to LLW/yr    |
|-----------|-------------------|-----------|-------------------|---------|-------------------|
| C         | 99                | <b>V</b>  | <b>54</b>         | Zn      | $1.1 \times 10^3$ |
| N         | $9.4 \times 10^4$ | <b>Cr</b> | <b>40</b>         | Y       | 21                |
| O         | $1.1 \times 10^4$ | <b>Mn</b> | <b>86</b>         | Zr      | $> 10^6$          |
| Mg        | 97                | Fe        | 59                | Nb      | $2.9 \times 10^5$ |
| Al        | 157               | Co        | 184               | Mo      | $8.7 \times 10^5$ |
| Si        | 58                | Ni        | $6.6 \times 10^5$ | Ta      | 41                |
| <b>Ti</b> | <b>10</b>         | Cu        | $1.3 \times 10^3$ | W       | 23                |

**Table 2**

Nominal and measured alloy compositions. Values are in at% with absolute standard errors shown.

| Nominal |       |       |    | Measured (EPMA)  |                  |                  |                 |
|---------|-------|-------|----|------------------|------------------|------------------|-----------------|
| V       | Cr    | Mn    | Ti | V                | Cr               | Mn               | Ti              |
| 60      | 20    | 20    | -  | $63.04 \pm 0.07$ | $20.58 \pm 0.03$ | $16.39 \pm 0.09$ | -               |
| 40      | 20    | 40    | -  | $39.40 \pm 0.24$ | $21.60 \pm 0.17$ | $39.01 \pm 0.08$ | -               |
| 40      | 40    | 20    | -  | $41.08 \pm 0.22$ | $43.20 \pm 0.35$ | $15.73 \pm 0.14$ | -               |
| 33.33   | 33.33 | 33.33 | -  | $32.80 \pm 0.28$ | $35.53 \pm 0.29$ | $31.68 \pm 0.04$ | -               |
| 33      | 33    | 33    | 1  | $42.03 \pm 0.03$ | $40.89 \pm 0.05$ | $15.69 \pm 0.07$ | $1.38 \pm 0.01$ |
| 32.67   | 32.67 | 32.67 | 2  | $35.82 \pm 0.16$ | $36.08 \pm 0.15$ | $25.10 \pm 0.11$ | $3.00 \pm 0.42$ |
| 32      | 32    | 32    | 4  | $34.53 \pm 0.02$ | $32.09 \pm 0.02$ | $27.92 \pm 0.02$ | $5.45 \pm 0.05$ |
| 30.67   | 30.67 | 30.67 | 8  | $35.84 \pm 0.18$ | $29.95 \pm 0.12$ | $25.52 \pm 0.03$ | $8.68 \pm 0.32$ |

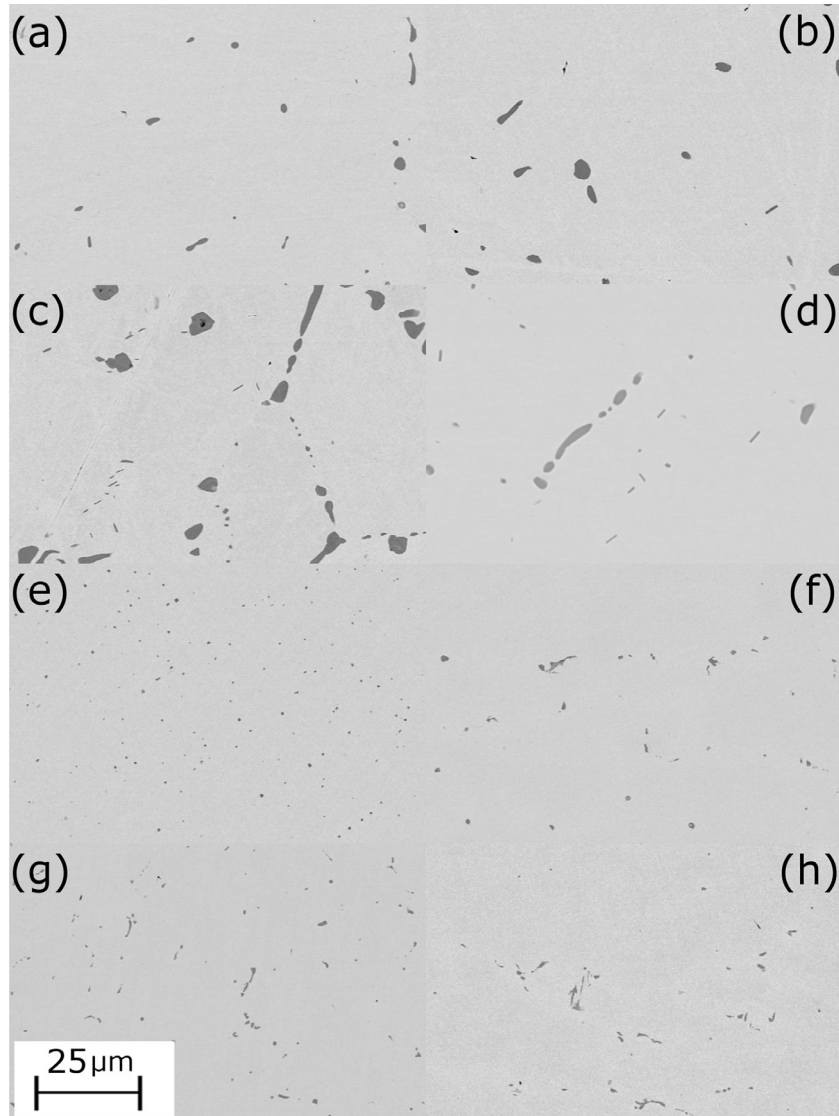


**Fig. 1.** Representative BSE images of alloy (a) V-20Cr-20Mn (b) V-20Cr-40Mn (c) V-40Cr-20Mn (d) V-Cr-Mn (e) V-Cr-Mn-1%Ti (f) V-Cr-Mn-2%Ti (g) V-Cr-Mn-4%Ti (h) V-Cr-Mn-8%Ti.

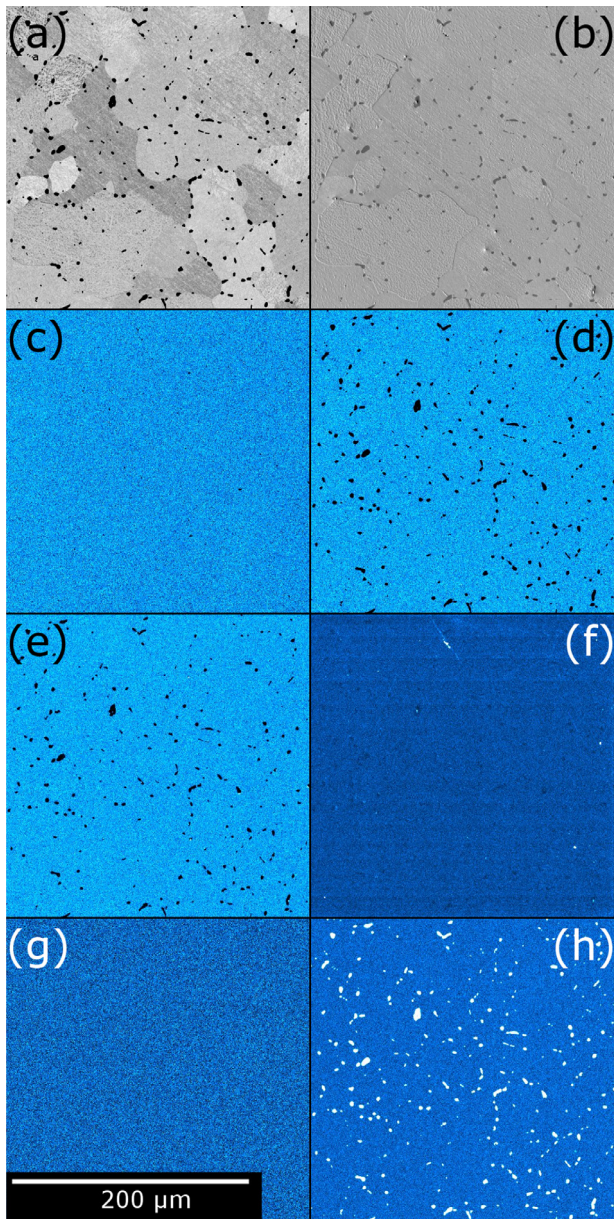


**Fig. 2.** WDS map of alloy V-40Cr-20Mn showing: (a) BSE image (b) secondary electron image (c) V (d) Cr (e) Mn (f) C (g) N (h) O.

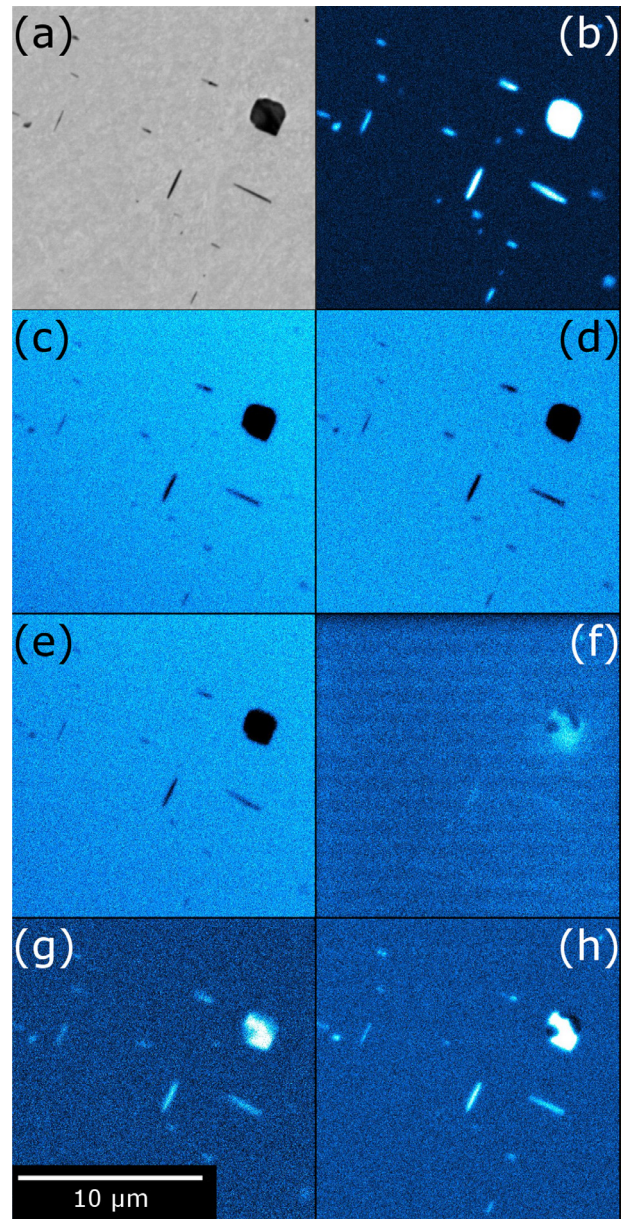


**Fig. 3.** WDS map of alloy V-Cr-Mn-8%Ti showing: (a) BSE image (b) Ti (c) V (d) Cr (e) Mn (f) C (g) N (h) O.

will allow for good creep performance at elevated temperatures in comparison to Fe-based alloys [6]. V and Cr show complete mutual solubility, forming a bcc phase at all compositions below the solidus [10]. A single bcc phase is considered highly desirable for adequate resistance to neutron irradiation swelling [11–13]. Additionally, Cr provides improved oxidation resistance in the binary system above around 30 wt% [10]. Such environmental resistance will be useful in limiting corrosion in service as well as in processing.

Mn was chosen as an extra element in working towards a HEA composition because the binary V-Mn and Cr-Mn diagrams show a good solubility of Mn in both Cr and V [14]. The V-Cr-Mn ternary is not well characterized, but the one ternary diagram available in the literature seems to agree that Mn should have good solubility in an alloy containing V and Cr [15]. Although the power of the entropic stabilisation effect in HEAs is disputed [16,17], the addition of Mn to a mixture of V and Cr will increase the configurational entropy of a solid solution of the elements and, therefore,

should increase its high-temperature stability. It was hoped that the stability of the solid solution would be increased sufficiently to allow for the introduction of higher concentration of elements like Ti (see below) with less propensity to form damaging intermetallics, such as Laves phases (which appear in the Ti-Mn and Ti-Cr binary [14]) or secondary solid solutions. Fe was not considered, despite being bcc and low-activation, as it is known to readily form undesirable sigma phases with Cr [18].

Finally, Ti was added to act as an impurity getter in a similar manner to the behaviour found in V-Cr-Ti alloys [3,19,20] and interstitial free steels [21]. A reduction of interstitial solute concentration is desirable as they are known to cause embrittlement in vanadium alloys [22]. However, high quantities of both Cr and Ti are known to embrittle vanadium alloys [23,24]. Furthermore, observation of the Ti-Mn and Ti-Cr binary phase diagrams suggests that Ti has low solubility in these two elements [14]. For these reasons, the amount of Ti added to the alloys was limited to 8 at%. Although the alloys studied here contain fewer elements than

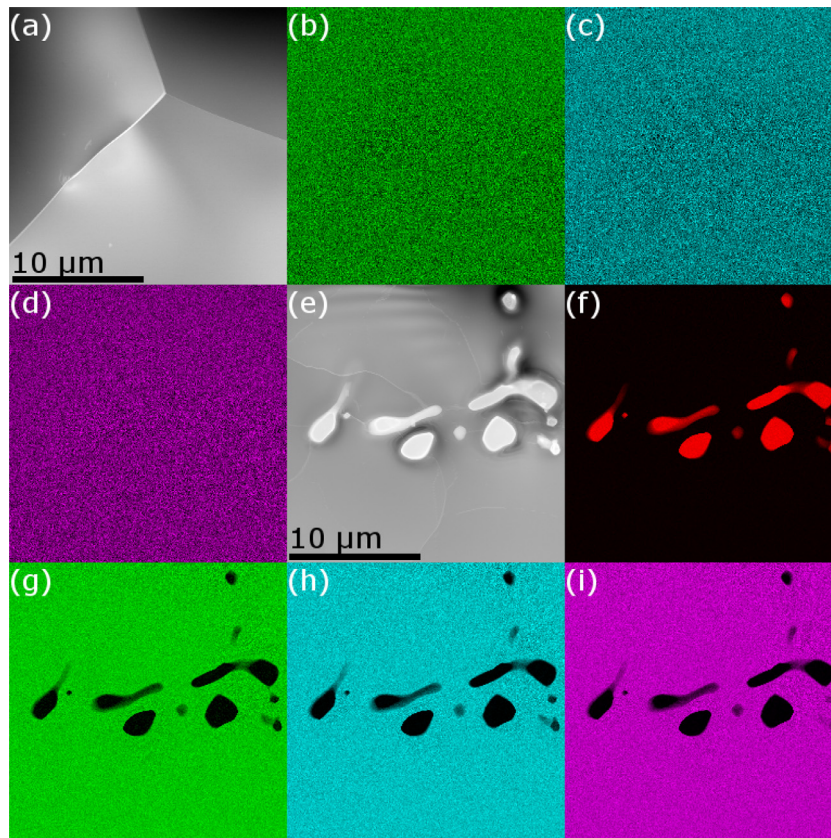


**Fig. 4.** Alloy V–Cr–Mn: (a) ADF image (b) V map (c) Cr map (d) Mn map. Alloy V–Cr–Mn–4%Ti precipitate: (e) ADF image (f) Ti map (g) V map (h) Cr map (i) Mn map.

necessary to be considered HEAs, and may instead be referred to as multi-principle element alloys (MPEAs), it is hoped they will contribute towards the development of true HEAs for fusion applications.

Eight alloys were fabricated as ingots weighing approximately 25 g using an arc melting process in an argon atmosphere. The ingots were inverted and remelted three times to ensure homogeneity. Sections of each ingot were cut off, wrapped in tantalum foil, and then encapsulated in a quartz ampoule backfilled with low pressure argon. These samples then underwent a homogenisation heat treatment at 1200 °C for 100 h, before quenching in water.

Secondary electron microscopy (SEM) specimens were prepared using standard metallographic techniques. The final polish was performed with an 0.06 μm oxide polishing suspension. Back scattered electron (BSE) images were obtained using a Zeiss Ultra55 microscope at 10 kV. Transmission electron microscopy (TEM) foils were produced by electropolishing punched sections of thin foils in a 5% perchloric acid-methanol solution with a temperature of –40 °C using a Tenupol 5 twin jet electropolisher at a voltage of 29 V. Further plasma polishing was performed using a Gatan PIPS II Model 695 polisher with conditions ranging from 1000 V for 20 min down to 100 V for two hours. A ThermoScientific Talos TEM with an accelerating voltage of 200 kV was used to produce annular dark field (ADF) images and energy dispersive X-ray (EDX) maps. Wavelength dispersive spectroscopy (WDS) was performed using a JEOL JXA-8530F FEG electron probe microanalyser (EPMA). Quantification was performed at 20 kV, 10 nA for Ti K $\alpha$ , V K $\alpha$ , Cr K $\alpha$  and Mn K $\beta$  standardised against pure metals. 100 composition measurements were randomly taken from an area 500 μm in radius for each sample. Overlap corrections were applied to the raw X-ray intensities where required (Ti K $\beta$  on V K $\alpha$ , V K $\beta$  on Cr

K $\alpha$ ) and corrected iteratively using the PAP phi-rho-Z matrix correction routine using NIST FFAST mass absorption coefficients. X-ray maps were conducted at 10 kV and 163 nA (V–40Cr–20Mn, Fig. 2) and 46 nA (V–Cr–Mn–8%Ti, Fig. 3). Vickers hardness measurements were taken with a load of 9.8 N and dwell time of 10 s using a Matsuzawa MMT-X indenter. Nine hardness measurements were made spaced 0.5 mm apart in a three by three grid formation.

WDS analysis suggests that there is a difference between the intended alloy composition and what is found in practice (see Table 2). In particular, the at% of Mn is lower than expected in all alloys. This is likely to be caused by the low vapour pressure of Mn, leading to evaporation during the arc melting process.

BSE images (Fig. 1) of the alloys show a microstructure consisting of a light grey matrix with darker precipitates. The precipitates found in the ternary alloys (Fig. 1(a)–(d)) are a mixture of larger, more rounded shapes which appear along grain boundaries, and smaller long and thin precipitates that are intragranular. The quaternary alloys have much finer precipitates (Fig. 1(e)–(h)). The matrix appeared as a single phase in all alloys. This was confirmed to be bcc ( $a = 2.90\text{--}3.04$  Å) through X-ray (see supplementary information) and TEM diffraction. These microstructures and lattice parameters are consistent with observations of a bcc Ti–V–Cr–Mn alloy with differing composition, used for hydrogen storage [25].

WDS was utilised to determine the composition of the matrix and precipitate phases. The matrix appeared to be a homogeneous mixture of the constituent metals in both the ternary (Fig. 2) and the quaternary alloys (Fig. 3). The main difference between the two types of alloy was in the composition of the precipitates. The ternary precipitates were depleted in Mn and Cr, and also

contained large amounts of oxygen. No segregation of other interstitial impurities (namely carbon and nitrogen) was observed. However, the precipitates in the Ti-containing alloys were extremely Ti rich relative to the matrix and were also enriched in all three impurity elements studied. This suggests that the addition of Ti to these alloys acts as a getter for these interstitial impurities, forming Ti-[C,O,N] type precipitates similar to those found in V-4Cr-4Ti. [3,19,20]

TEM was used to check for smaller scale elemental segregation as shown in Fig. 4. No segregation was found, indicating a homogeneous bcc phase across all lengthscales. Diffraction patterns (see supplementary information) indicated that the precipitates in the ternary alloys were fcc with a lattice parameter of approximately 8.38 Å. This is a close match with the spinel  $MnV_2O_4$  [26] which suggests a similar structure, perhaps with slightly altered stoichiometry. Diffraction patterns of the quaternary alloy precipitates indicate an fcc structure with a lattice parameter of approximately 4.16 Å, which is consistent with the Ti-[C,O,N] phase found in V-4Cr-4Ti alloys [19]. As all the precipitates found in this study are formed from impurity elements, there is no indication that these alloys would not form a single bcc phase if interstitial impurity content was lower.

Hardness values were found to range from 348 to 456 HV in the homogenised state (see supplementary information). Hardness decreased slightly after homogenisation for all alloys. The Ti containing alloys were all harder than their equiatomic ternary equivalent, V-Cr-Mn, which may indicate the solute strengthening caused by introducing Ti [23,24] is the more dominant effect compared to the softening from gettering interstitial impurities [22]. A high ductile-to-brittle transition temperature and embrittlement by interstitial elements are foreseeable issues with these alloys, as they are with most refractory-based alloys. Hence, in order to assess their suitability for manufacture and service, larger-scale mechanical property and processability investigations are needed alongside long-term ageing experiments.

To summarise, this study has found that a suite of alloys fabricated from low-activation elements consists of a single bcc phase, with precipitates forming from interstitial impurity elements. The results are promising for the development of high-entropy alloys for use in fusion applications due to the observation of only a single metallic matrix phase after homogenisation. Such microstructures provide an excellent launchpad for the future development of specialist alloys for fusion applications.

## Acknowledgments

The authors acknowledge the use of the Department of Materials X-ray Diffraction Suite at the University of Manchester and for the technical support, advice and assistance provided by Dr. John E. Warren. The authors would also like to Dr. Mark Gilbert for fruitful discussions regarding the activation properties of elements. The authors acknowledge funding from the EPSRC Centre for Doctoral Training in Fusion Energy [grant EP/L01663X/1] as well as

EPSRC grant EP/R021546/1. This work has been part-funded by the RCUK Energy Programme [grant number EP/T012250/1]. To obtain further information on the data and models underlying this paper please contact [PublicationsManager@ukaea.uk](mailto:PublicationsManager@ukaea.uk).

## Supplementary material

Supplementary material associated with this article can be found, in the online version, at doi:[10.1016/j.scriptamat.2019.09.028](https://doi.org/10.1016/j.scriptamat.2019.09.028).

## References

- [1] A. Raffray, M. Akiba, V. Chuyanov, L. Giancarli, S. Malang, J. Nuclear Mater. 307–311 (2002) 21–30, doi:[10.1016/S0022-3115\(02\)01174-1](https://doi.org/10.1016/S0022-3115(02)01174-1).
- [2] M. Gilbert, T. Eade, T. Rey, R. Vale, C. Bachmann, U. Fischer, N. Taylor, Nuclear Fus. 59 (7) (2019) 076015, doi:[10.1088/1741-4326/ab154e](https://doi.org/10.1088/1741-4326/ab154e).
- [3] T. Muroga, J. Chen, V. Chernov, R. Kurtz, M. Le Flem, J. Nuclear Mater. 455 (1) (2014) 263–268, doi:[10.1016/j.jnucmat.2014.06.025](https://doi.org/10.1016/j.jnucmat.2014.06.025).
- [4] S. Zinkle, J.-L. Boutard, D. Hoelzer, A. Kimura, R. Lindau, G. Odette, M. Rieth, L. Tan, H. Tanigawa, Nuclear Fus. 57 (9) (2017) 092005, doi:[10.1088/1741-4326/57/9/092005](https://doi.org/10.1088/1741-4326/57/9/092005).
- [5] A. Rowcliffe, L. Garrison, Y. Yamamoto, L. Tan, Y. Katoh, Fus. Eng. Des. 135 (2018) 290–301, doi:[10.1016/j.fusengdes.2017.07.012](https://doi.org/10.1016/j.fusengdes.2017.07.012).
- [6] S.J. Zinkle, N.M. Ghoniem, Fus. Eng. Des. 51–52 (2000) 55–71, doi:[10.1016/S0920-3796\(00\)00320-3](https://doi.org/10.1016/S0920-3796(00)00320-3).
- [7] A. Ayyagari, R. Sallloom, S. Muskeri, S. Mukherjee, Materialia 4 (2018) 99–103, doi:[10.1016/j.mtl.2018.09.014](https://doi.org/10.1016/j.mtl.2018.09.014).
- [8] B. Gludovatz, A. Hohenwarter, D. Catoor, E.H. Chang, E.P. George, R.O. Ritchie, Science 345 (6201) (2014) 1153–1158, doi:[10.1126/science.1254581](https://doi.org/10.1126/science.1254581).
- [9] K. Jin, C. Lu, L. Wang, J. Qu, W. Weber, Y. Zhang, H. Bei, Scr. Mater. 119 (2016) 65–70, doi:[10.1016/j.scriptamat.2016.03.030](https://doi.org/10.1016/j.scriptamat.2016.03.030).
- [10] O.N. Carlson, A.L. Eustice, AMES Laboratory Technical Reports 12 (1959) [http://lib.dr.iastate.edu/ameslab\\_isreports/12](http://lib.dr.iastate.edu/ameslab_isreports/12).
- [11] F. Garner, M. Toloczko, B. Sencer, J. Nuclear Mater. 276 (1–3) (2000) 123–142, doi:[10.1016/S0022-3115\(99\)00225-1](https://doi.org/10.1016/S0022-3115(99)00225-1).
- [12] S. Zinkle, Compreh. Nuclear Mater. (2012) 65–98, doi:[10.1016/B978-0-08-056033-5.00003-3](https://doi.org/10.1016/B978-0-08-056033-5.00003-3).
- [13] S. Zinkle, L. Snead, Ann. Rev. Mater. Res. 44 (1) (2014) 241–267, doi:[10.1146/annurev-matsci-070813-113627](https://doi.org/10.1146/annurev-matsci-070813-113627).
- [14] T. Massalski, Binary Alloy Phase Diagrams, ASM International, 1986.
- [15] A. Klopotov, I. Kurzina, A. Potekaev, A. Ustinov, T. Dement, L. Kazantseva, E. Marchenko, N. Karakchieva, MATEC Web Conf. 243 (2018) 00014, doi:[10.1051/mateconf/201824300014](https://doi.org/10.1051/mateconf/201824300014).
- [16] E.J. Pickering, N.G. Jones, Int. Mater. Rev. 6608 (May) (2016) 1–20, doi:[10.1080/09506608.2016.1180020](https://doi.org/10.1080/09506608.2016.1180020).
- [17] D. Miracle, O. Senkov, Acta Mater. 122 (2017) 448–511, doi:[10.1016/j.actamat.2016.08.081](https://doi.org/10.1016/j.actamat.2016.08.081).
- [18] O.K. von Goldbeck, Iron-Chromium Fe–Cr, Springer Berlin Heidelberg, Berlin, Heidelberg, pp. 31–34, doi:[10.1007/978-3-662-08024-5\\_17](https://doi.org/10.1007/978-3-662-08024-5_17).
- [19] D. Hoelzer, Technical Report, Oak Ridge National Laboratory, 1999.
- [20] T. Nagasaka, N. Heo, T. Muroga, M. Imamura, Fus. Eng. Des. 61–62 (2002) 757–762, doi:[10.1016/S0920-3796\(02\)00258-2](https://doi.org/10.1016/S0920-3796(02)00258-2).
- [21] S. Hoile, Mater. Sci. Technol. 16 (10) (2000) 1079–1093, doi:[10.1179/026708300101506902](https://doi.org/10.1179/026708300101506902).
- [22] J.M. Chen, V.M. Chernov, R.J. Kurtz, T. Muroga, J. Nuclear Mater. 417 (1–3) (2011) 289–294, doi:[10.1016/j.jnucmat.2011.02.015](https://doi.org/10.1016/j.jnucmat.2011.02.015).
- [23] B. Loomis, H. Chung, L. Nowicki, D. Smith, J. Nuclear Mater. 212–215 (94) (1994) 799–803, doi:[10.1016/0022-3115\(94\)90166-X](https://doi.org/10.1016/0022-3115(94)90166-X).
- [24] H.M. Chung, B.A. Loomis, D.L. Smith, J. Nuclear Mater. 239 (1–3) (1996) 139–156, doi:[10.1016/S0022-3115\(96\)00676-9](https://doi.org/10.1016/S0022-3115(96)00676-9).
- [25] T. Fuda, A. Kamegawa, Y. Tominaga, T. Kuriwa, K. Matsumoto, T. Tamura, H. Takamura, M. Okada, J. Alloys Compounds 330–332 (2002) 522–525, doi:[10.1016/S0925-8388\(01\)01544-4](https://doi.org/10.1016/S0925-8388(01)01544-4).
- [26] R. Plumier, Comptes Rendus Hebdomadaires des Seances de l'Academie des Sciences 255 (1962) 2244–2246.